

Electrical tuning of tin-vacancy centers in diamond

Shahriar Aghaeimeibodi,^{1,2,*} Daniel Riedel,^{1,*} Alison E. Rugar,^{1,*} Constantin Dory,¹ and Jelena Vučković¹

¹*E. L. Ginzton Laboratory, Stanford University, Stanford, CA 94305, USA*

²*shahriar@stanford.edu*

Group-IV color centers in diamond have attracted significant attention as solid-state spin qubits because of their excellent optical and spin properties. Among these color centers, the tin-vacancy (SnV^-) center is of particular interest because its large ground-state splitting enables long spin coherence times at temperatures above 1 K. However, color centers typically suffer from inhomogeneous broadening, which can be exacerbated by nanofabrication-induced strain, hindering the implementation of quantum nodes emitting indistinguishable photons. Although strain and Raman tuning have been investigated as promising techniques to overcome the spectral mismatch between distinct group-IV color centers, other approaches need to be explored to find methods that can offer more localized control without sacrificing emission intensity. Here, we study electrical tuning of SnV^- centers in diamond via the direct-current Stark effect. We demonstrate a tuning range beyond 1.7 GHz. We observe both quadratic and linear dependence on the applied electric field. We also confirm that the tuning effect we observe is a result of the applied electric field and is distinct from thermal tuning due to Joule heating. Stark tuning is a promising avenue toward overcoming detunings between emitters and enabling the realization of multiple identical quantum nodes.

I. INTRODUCTION

Group-IV color centers in diamond have emerged as promising candidates for the implementation of quantum networks [1, 2] because they retain their optical coherence when integrated with nanophotonic devices [3–6]. These color centers are inversion-symmetric and thus exhibit a vanishingly small permanent electric dipole moment, which mitigates the influence of electric field fluctuations and results in a high frequency stability of their optical transitions [7]. Most notably, the negatively charged silicon-vacancy (SiV^-) center in diamond has been used to implement several quantum information processing applications [8–10]. However, the relatively small ground-state splitting (GSS) of SiV^- centers restricts the long spin coherence of this emitter to millikelvin temperatures. On the other hand, the negatively charged tin-vacancy (SnV^-) center comprises a heavier group-IV element in a split-vacancy configuration [11–16]. The comparatively large GSS of SnV^- centers facilitates long spin coherence times at liquid helium temperatures (>1 K) because of the reduced phonon-induced decoherence [17].

Quantum networks require multiple identical quantum nodes that emit indistinguishable photons. A significant challenge for solid-state quantum emitters is that each individual emitter experiences a slightly different strain environment, leading to an inhomogeneous distribution of their optical transition frequencies. Because of the aforementioned inversion symmetry, the spread of optical transition frequencies of group-IV color centers can be very narrow in a low-strain environment [18, 19]. Nevertheless, in diamond nanostructures, fabrication-induced strain produces a slightly larger inhomogeneous broaden-

ing (< 15 GHz) [5]. Therefore, to achieve indistinguishable emission from distinct color centers, precise tuning of optical transition frequencies is essential. Raman [3, 20] and magnetic field [8] tuning have been employed to control the emitter frequency over ranges comparable to this spread. Those techniques, however, either strongly reduce the photon detection rate or cannot be applied locally on several emitters on the same chip to compensate their frequency detuning. Electromechanical tuning offers a potential solution and has enabled the tuning of the transition frequency of waveguide-coupled SiV^- centers by tens of GHz [6, 21]. This technique, however, is limited to freestanding waveguide structures. Applying an electric field could potentially offer an alternative tuning mechanism through the Stark effect. However, because of the predicted first order insensitivity of transitions to electric fields, this approach has not been realized.

In this Letter, we investigate the electric field susceptibility of SnV^- centers in diamond. We demonstrate reversible tuning of the transition wavelength by more than 1.7 GHz, which is ~ 57 times the natural linewidth of ~ 30 MHz [17]. We measure linear and quadratic Stark effect coefficients for SnV^- centers to be several orders of magnitude smaller than those of non-inversion-symmetric color centers. The remaining linear shift in some emitters may originate from the relatively high strain in our diamond sample, which we infer from the large distribution of transition frequencies (~ 270 GHz) of SnV^- centers in this sample, as previously characterized in Ref. 12. Furthermore, we perform careful control experiments to distinguish the tuning achieved through the Stark effect from that resulting from parasitic heating of the diamond sample. Our results, when combined with an initial pre-selection of emitters for nearby transition frequencies, could enable the realization of multi-emitter quantum information processing applications using diamond color centers.

* These authors contributed equally to this work.

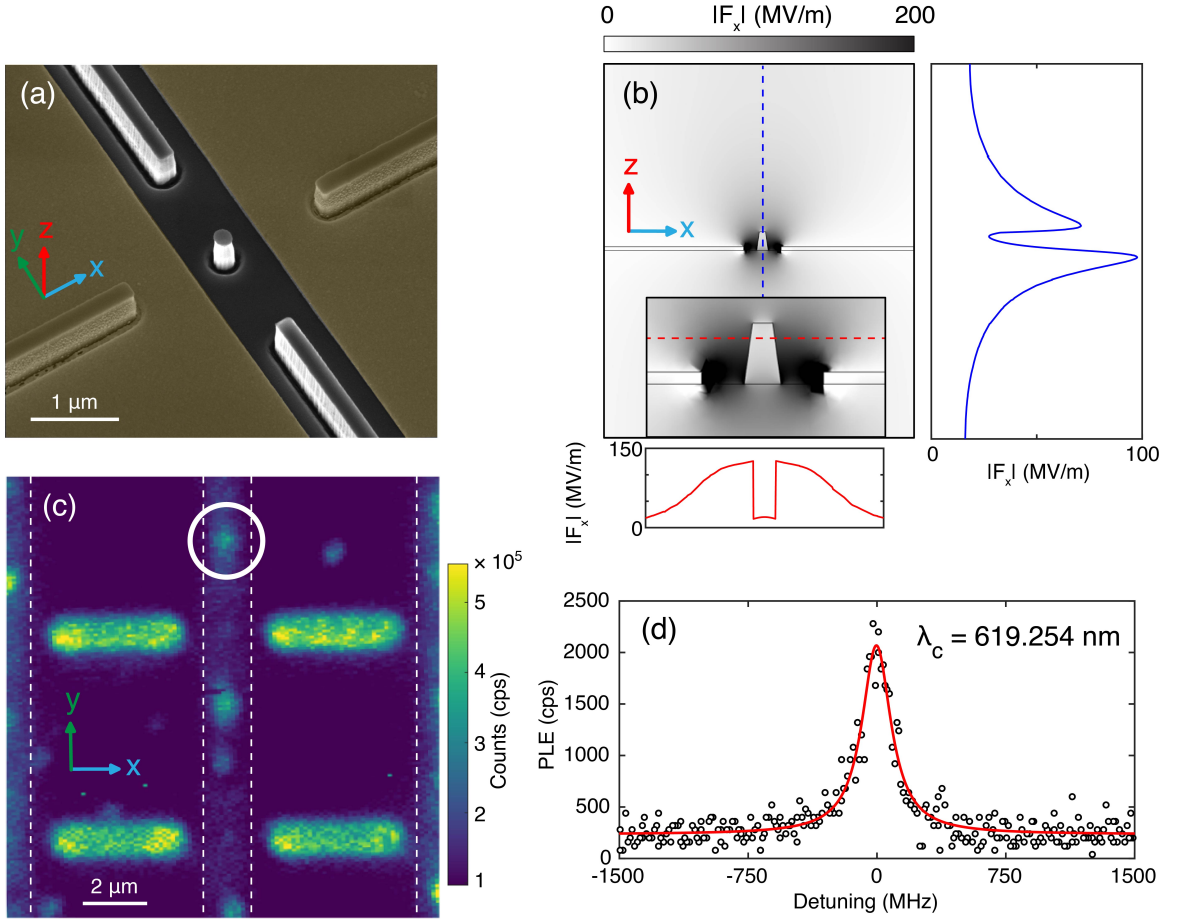


FIG. 1. Device fabrication and characterization. **(a)** Scanning electron microscope image of fabricated diamond structure and electrodes. Electrodes are highlighted by false-color gold. **(b)** Simulated electric field magnitude along the x-direction ($|F_x|$) for an applied voltage of 200 V across the electrodes. Inset shows close up of $|F_x|$ in mesa. Electric fields along the dashed blue and red lines are plotted in the panels to the right ($|F_x(z)|$) and below ($|F_x(x)|$), respectively. **(c)** Photoluminescence map of the device. One of the SnV⁻ centers that we study in this work (E1) is circled in white. Edges of electrodes are demarcated by white dashed lines. **(d)** Photoluminescence excitation measurement performed on the C transition of the marked SnV⁻ center in (c) at zero applied electric field. Lorentzian fit (red curve) to data (black circle) reveals a linewidth of 194 ± 12 MHz.

II. FABRICATION AND CHARACTERIZATION

We begin our fabrication process with an electronic-grade, single-crystal diamond plate from Element Six. The chip is cleaned in a boiling tri-acid (1:1:1 sulfuric/nitric/perchloric acids) solution. We then remove the top 300 nm of diamond with an oxygen (O_2) plasma etch. SnV⁻ centers are generated via $^{120}\text{Sn}^+$ ion implantation (370 keV, $2 \times 10^{11} \text{ cm}^{-2}$) followed by vacuum annealing at 800°C for 30 minutes and 1100°C for 90 minutes. Based on Stopping Range of Ions in Matter (SRIM) simulations [22], we expect the depth of our SnV⁻ centers to be ~ 90 nm.

After generating SnV⁻ centers in diamond, we fabricate nanopillars and mesas to easily identify single SnV⁻ centers and to increase the photon extraction efficiency. We grow 200 nm of silicon nitride (Si_xN_y) via low-

pressure chemical vapor deposition. We pattern square arrays of circles (pillars) separated by rectangles (mesas) in hydrogen silsesquioxane FOx-16 via electron-beam (e-beam) lithography. The circles range in diameter from 140 nm to 300 nm. The rectangles are $0.2 \mu\text{m} \times 2.5 \mu\text{m}$. The pattern is transferred into the Si_xN_y film by a SF_6 , CH_4 , and N_2 reactive ion etch. Using the Si_xN_y layer as an etch mask, we perform an O_2 plasma etch to fabricate 500-nm tall diamond nanopillars and mesas. Finally, the etch mask is removed by soaking the sample in hydrofluoric acid.

We then fabricate parallel electrodes around a column in an array of nanopillars to produce an electric field along the [100] direction. The 4- μm wide electrodes are placed 1 μm apart. The electrodes are created via metal liftoff. Poly(methyl methacrylate) (PMMA) is patterned via e-beam lithography. Then 5 nm of Ti followed

by 30 nm of Au are deposited by e-beam evaporation. The remaining PMMA is lifted off in acetone. A scanning electron microscope image of the resulting diamond structures and metal electrodes is shown in Fig. 1(a).

We use the finite element method (COMSOL) to simulate the electric field inside a pillar or a mesa. Fig. 1(b) shows the simulated magnitude of the electric field along the x direction ($|F_x|$) when 200 V is applied across the electrodes. The inset is a close-up view of the field distribution around the mesa, indicating a lower magnitude in the mesa compared to the bulk region. The right panel in Fig. 1(c) is a vertical line cut through the center of a diamond mesa, showing $|F_x|$ as a function of z position, while the bottom panel shows $|F_x|$ as a function of x at the estimated implantation depth. The electric field magnitude is a factor of three smaller at ~ 90 nm below the top of the mesa, than at the surface of diamond for a bulk region.

We perform the optical characterization of SnV^- centers in this sample at ~ 5 K in a cryostat (Montana Instruments Cryostation). Using a home-built scanning confocal microscope setup, we scan a 532-nm continuous-wave laser across our sample and collect the emission into the SnV^- center zero-phonon line with a (620 ± 14) -nm bandpass filter placed in front of a multi-mode fiber to acquire a photoluminescence (PL) map of the region (Fig. 1(c)).

At 5 K, the SnV^- center has two dominant zero-phonon line transitions often referred to as the C and D transitions [14]. These transitions are centered around 620 nm, and in unstrained SnV^- centers the C transition is typically ~ 850 GHz higher in energy than the D transition. We perform a photoluminescence excitation (PLE) measurement on the C transition of the emitter circled in Fig. 1(c), which we will refer to as E1, to characterize its resonant frequency and linewidth. We scan the wavelength of a tunable laser (MSquared SolsTiS and External Mixing Module) around the transition wavelength and collect the emission into the phonon sideband (PSB) with a 638-nm long-pass filter and a 700-nm short-pass filter placed before a multi-mode collection fiber. When the laser passes through resonance with the C transition, a peak in the PSB photon counts occurs. To this peak, shown in Fig. 1(e), we fit a Lorentzian curve to find the center wavelength 619.254 nm and linewidth (194 ± 12) MHz.

III. VOLTAGE-DEPENDENT PHOTOLUMINESCENCE EXCITATION

To investigate the behavior of the SnV^- center in the presence of an electric field, we apply a direct-current (DC) voltage to the electrodes using a high-voltage power supply (Stanford Research Systems PS325). Fig. 2 shows consecutive PLE scans of the color center E1 as we vary the applied voltage. We observe a reversible redshift in the resonant frequency of the SnV^- center for both po-

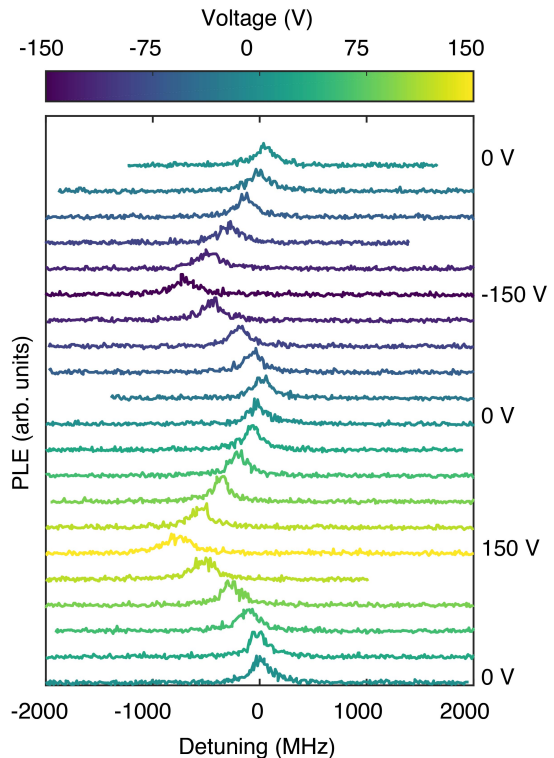


FIG. 2. PLE measurements acquired consecutively at different applied voltages. The PLE resonance reproducibly shifts as a function of applied voltage.

larities of the electric field. Repeatable tuning of the emission frequency confirms that there is no damage to the SnV^- even at extremely high electric fields of ~ 50 MV/m.

To gain a better understanding of the origin of the shift for single SnV^- centers, we fit the PLE data in Fig. 2 to a Lorentzian function to extract the shift, linewidth, and the intensity of the signal as we vary the electric field. We approximate the electric field at the location of the emitter using the Lorentz approximation $F_{\text{Local}} = F_{\text{ext}}(\epsilon + 2)/3$, where F_{ext} is the field extracted from the COMSOL simulations and ϵ is the dielectric constant of diamond [23].

A. Quadratic shift

Fig. 3(a) shows the extracted shift of the resonance frequency of the SnV^- center E1 as a function of the applied electric field. We fit the extracted shift (ΔE) in Fig. 3(a) to a quadratic function of the form $\Delta E = -\Delta\mu F_{\text{Local}} - 1/2\Delta\alpha F_{\text{Local}}^2$ where $\Delta\mu$, and $\Delta\alpha$ are the change in dipole moment and polarizability between the excited and ground states. An inversion-symmetric defect such as the SnV^- center is expected to have a vanishing $\Delta\mu$, making polarizability $\Delta\alpha$ the predominant coefficient. From the fit, we extract $\Delta\mu = (0.97 \pm 0.57)$ MHz/(MV/m) which corresponds to $(1.9 \pm 1.1) \times$

10^{-4} D. This value is several orders of magnitude smaller than that of non-inversion-symmetric color centers such as nitrogen-vacancy (NV^-) centers in diamond [23] and silicon vacancy (V_{Si}) centers in silicon carbide [24]. We also obtain $\Delta\alpha = (0.55 \pm 0.03) \text{ MHz}/(\text{MV}/\text{m})^2$ which converts to a polarizability volume $\Delta\alpha/(4\pi\epsilon_0) = 3.28 \pm 0.18 \text{ \AA}^3$. We note that this polarizability volume is four orders of magnitude smaller and has the opposite sign compared to that of NV^- centers in diamond [23]. Most emitters have a positive polarizability because excited states tend to be more polarizable than ground states [23].

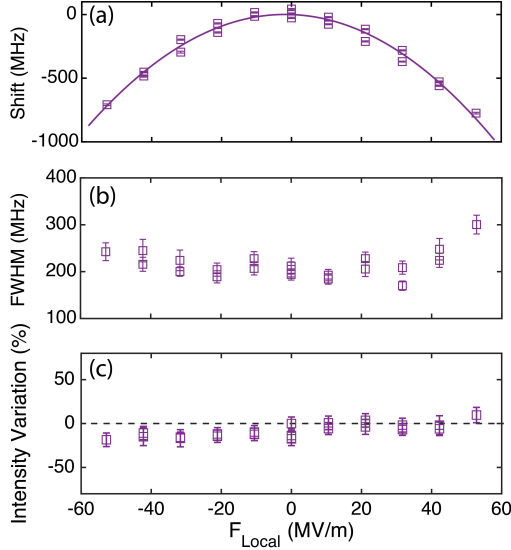


FIG. 3. Characterizing the Stark effect in a single SnV^- center (E1) with predominantly quadratic shift. **(a)** Stark shift extracted from Lorentzian fits to the PLE data in Fig. 2 as a function of the applied electric field F_{Local} . The shifts show a mostly quadratic dependence on the applied field with $\Delta\mu = (1.9 \pm 1.1) \times 10^{-4}$ D and $\Delta\alpha/(4\pi\epsilon_0) = (3.28 \pm 0.18) \text{ \AA}^3$ obtained from the fit. **(b)** Full width at half-maximum (FWHM) of the PLE signal of the same emitter as a function of F_{Local} . At high electric fields, the linewidth increases to ~ 300 MHz from its original value ~ 200 MHz value at zero field. **(c)** Integrated intensity of the PLE data as a function of F_{Local} . We observe $< \pm 20\%$ variation in the integrated intensity of the PLE signal for the entire range of the electric field.

Fig. 3(b) shows the linewidth of the SnV^- center obtained from the full width at half-maximum (FWHM) of the Lorentzian fits to the PLE data as a function of applied electric field. We observe an increase in the linewidth from the zero-field value of ~ 200 MHz to 300 MHz for the highest electric field. We attribute this increase in linewidth to Joule heating because of the leakage current, as we discuss later. Fig. 3(c) displays the variation in integrated intensity of the PLE signal as a function of the applied electric field. We observe less than $\pm 20\%$ variation in the integrated intensity of the

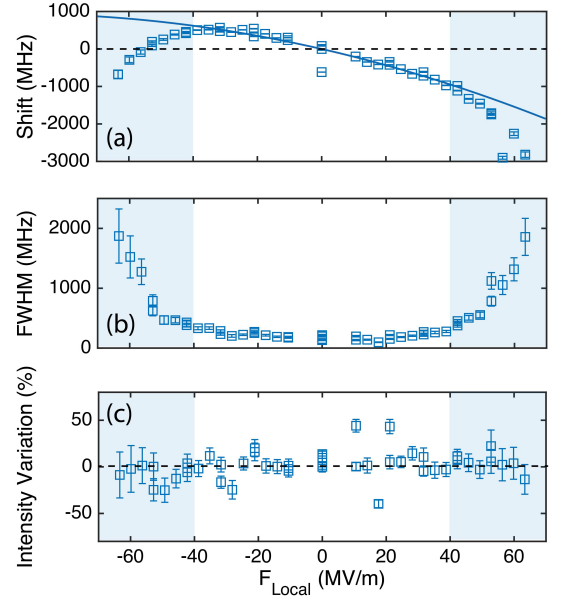


FIG. 4. Characterizing the Stark effect in a single SnV^- center (E2) with predominantly linear shift. **(a)** Stark shift extracted from Lorentzian fits to the voltage-dependent PLE spectra of E2. The shifts show a mostly linear dependence on the applied field with $\Delta\mu = (3.9 \pm 0.4) \times 10^{-3}$ D and $\Delta\alpha/(4\pi\epsilon_0) = (1.19 \pm 0.89) \text{ \AA}^3$ obtained from the fit. **(b)** FWHM of the PLE signal of the same emitter as a function of electric field F_{Local} . At high electric fields (shaded area), the linewidth rapidly increases. We attribute this significant line broadening to Joule heating through leakage current, as we will discuss later in the text. **(c)** Integrated intensity of the PLE data as a function of F_{Local} . We observe $< \pm 45\%$ variation in the integrated intensity of the PLE signal for the entire range of the electric field.

signal for a large range of applied electric fields, indicating the potential of this technique as a means to tune SnV^- centers into resonance with each other.

B. Linear shift

We study the electric-field dependence of transition frequency for several other SnV^- centers. Although a quadratic shift is expected because of the inversion-symmetric structure of this color center, some emitters exhibit a mostly linear shift in transition frequency as a function of applied electric field. Figs. 4(a)-(c) respectively display the extracted shift, linewidth, and intensity variation of PLE spectra for an emitter with mostly linear shift (E2). At local electric field magnitudes greater than 40 MV/m (shaded blue regions), we observe a red-shift in the transition frequency and a sharp increase in the SnV^- linewidth regardless of the field polarity. We attribute this linewidth broadening to Joule heating through leakage current. We observed that the onset voltage for the Joule heating decreased over time, indi-

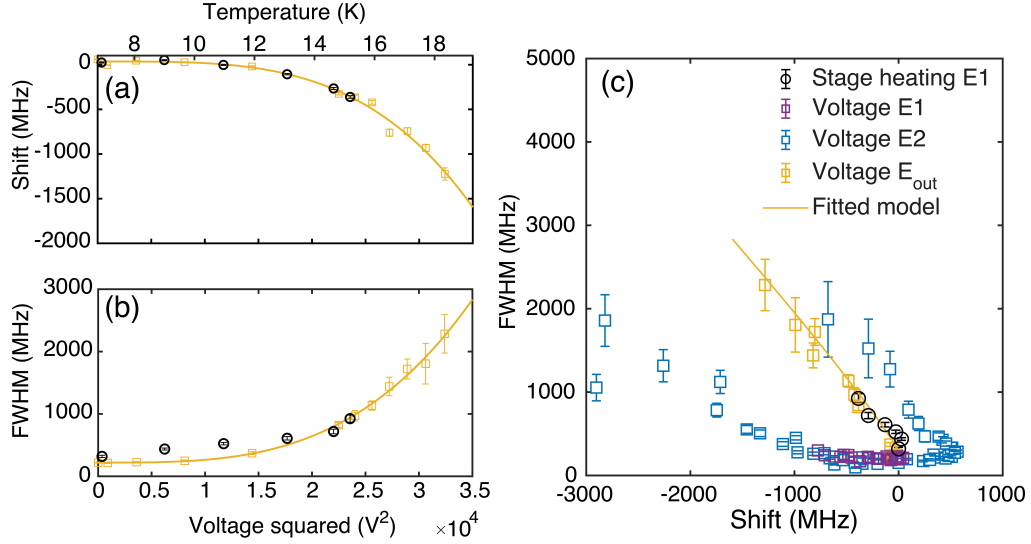


FIG. 5. A comparison between Stark and temperature tuning. **(a)** Effect of Joule heating on resonant frequency shift of an emitter E_{out} located outside the electrodes. A power law model (yellow curve) is fit to the data (yellow squares), indicating a dependence on temperature ($T \propto V^2$), $T^{3.6 \pm 0.7}$. Black circles correspond to the temperature-dependent shift for E1 obtained from heating the sample. **(b)** Effect of Joule heating on the FWHM of E_{out}. A power law model (curve) is fit to the data (squares) with a $T^{3.3 \pm 0.4}$ dependence on temperature. Black circles correspond to the temperature-dependent FWHM for E1 obtained from heating the sample. **(c)** FWHM as a function of the extracted shift in the PLE signal for three different tuning methods. Purple (Blue) squares correspond to the Stark tuning of the emitter E1 (E2). Yellow squares show the data for E_{out}. Black circles represent the tuning of emitter E1 obtained by heating the sample stage. The similar behaviors of the black circles and yellow squares confirm that they both originate from heating and are fundamentally different from the shift obtained by the Stark effect. The yellow solid line is the curve resulting from the fitted models from panels (a) and (b) plotted against each other.

No.	λ_C (nm)	Linewidth (MHz)	$\Delta\mu$ (10^{-3} D)	$\Delta\alpha/(4\pi\epsilon_0)(\text{\AA}^3)$	GSS (GHz)	Shift (GHz)	Type
E1	619.254	194 ± 12	0.19 ± 0.11	3.28 ± 0.18	819.6	0.82	Quadratic
E2	619.236	132 ± 6	3.9 ± 0.4	1.19 ± 0.89	982.9	1.68	Linear
E3	619.255	126 ± 6	-0.5 ± 0.5	3.8 ± 1.1	947.7	0.59	Quadratic
E4	619.500	160 ± 9	-8.2 ± 1.8	5.36 ± 4.05	989.4	1.73	Linear

TABLE I. Linear and quadratic Stark effect coefficients of single SnV⁻ centers. λ_C (wavelength of C transition) and linewidth are obtained from Lorentzian fits to the PLE spectra at zero electric field. $\Delta\mu$ and $\Delta\alpha$ are Stark coefficients resulting from the same quadratic fit as in Fig. 3(a). The energy difference between the C and D transitions measured through PL spectroscopy gives the GSS. We define the useful shifting range as the largest tuning range achievable without broadening the linewidth by more than a factor of 2. Transition frequencies of E1 and E3 are < 1 GHz apart.

cating a possible damaged or burned area on the electrodes. In order to extract the Stark parameters without distortions caused by heating, we excluded the data in the shaded region for the fit. The solid blue line in Fig. 4(a) is a fit to the same model as in Fig. 3(a) with extracted parameters $\Delta\mu = (3.9 \pm 0.4) \times 10^{-3}$ D and $\Delta\alpha/(4\pi\epsilon_0) = (1.19 \pm 0.89) \text{\AA}^3$. This $\Delta\mu$ is more than an order of magnitude larger than that of E1 studied in Fig. 3 and could be due to broken inversion symmetry in a strained SnV⁻ center. The larger GSS in E2 (~ 983 GHz) compared to E1 (~ 820 GHz) is another indication of a higher strain environment for E2 [25]. We repeat this measurement for multiple SnV⁻ centers between the electrodes and report the extracted parameters in Table I.

C. Joule heating

To confirm that the observed Stark shift is not related to Joule heating of the color center because of the leakage current, we perform two additional control experiments: we tune a SnV⁻ center either (1) by applying a voltage across the electrodes while measuring an emitter outside of the electrode region (E_{out}) or (2) by heating the sample and studying E1. We extract the linewidth and resonance frequency of the SnV⁻ centers through PLE measurements. In our first control experiment, we study another emitter E_{out} that is located outside of the electrode region. Because E_{out} is sufficiently far from the electrodes, the DC electric field vanishes and any shift in frequency for this emitter should be due to leakage current, Joule heating, and the high thermal conductivity of diamond.

In Figs. 5(a) and (b), we plot the shift and FWHM as functions of the square of the voltage applied across the electrodes (V^2). With Joule heating, the induced temperature change is proportional to the applied voltage squared ($T \propto V^2$), so we use these data to characterize the temperature-dependent behavior of E_{out} . We fit a power law model to the E_{out} data of Figs. 5(a) and (b). From these fits, we find that the thermally induced shift is proportional to $T^{3.6 \pm 0.7}$ and $\text{FWHM} \sim T^{3.3 \pm 0.4}$. This temperature dependence of frequency and FWHM is consistent with previous studies of SiV^- centers [26]. For the second control experiment, we tune the energy of the SnV^- center studied in Fig. 3 (E1) by heating the cryostat up to ~ 20 K. We plot the detuning and FWHM data of E1 as a function of temperature in Figs. 5(a) and (b). We use the extracted shift of the heated E1 and E_{out} to calibrate the proportionality constant between V^2 and T .

In Fig. 5(c), we plot FWHM as a function of frequency shift for our two control experiments as well as E1 (Fig. 3) and E2 (Fig. 4). We also plot the modeled FWHM against the modeled shift from Figs. 5(a) and (b) as a solid yellow line. The data from the two temperature-tuning control experiments are consistent with each other and exhibit a vastly different behavior from the electrically tuned E1. Furthermore, we can see that at large detunings the slope of the E2 data increases dramatically, approaching the behavior of the thermally tuned emitters. These comparisons prove that while leakage current through electrodes can, in principle, cause Joule heating and broadening of the PLE data, the Stark shifts presented in Figs. 3(a) and 4(a) are not influenced by this effect until very high local fields exceeding 40 MV/m.

IV. CONCLUSIONS

We have examined the response of the frequency of the C transition of SnV^- centers in diamond to externally applied electric fields. We can shift the transition frequency by more than 1.7 GHz without introducing a significant broadening of the transition linewidth. We investigate several SnV^- centers and observe both linear and quadratic dependencies of the shift on the applied electric field. While a quadratic dependence is expected based on the defect's inversion symmetry, we attribute the linear shift to a small, strain-induced dipole moment. We find changes in dipole moment and polarizability volume between the excited and ground states of up to $\Delta\mu = -8.2 \times 10^{-3}$ D and $\Delta\alpha/(4\pi\epsilon_0) = 5.4 \text{ \AA}^3$, respectively. Furthermore, we confirm that the observed shift is due to the Stark effect and is distinct from any heating effects by comparing the linewidth versus frequency shift of the emitter when a voltage is applied to that when the stage is heated.

Stark tuning can be used to tune the optical frequency of remote emitters and to control the degree of indistinguishability in two-photon interference experiments of pre-selected emitters [27–31]. This technique, which re-

cently enabled the first demonstration of linking three remote NV^- centers in a quantum network [32], may also be applied to group-IV color centers. Group-IV color centers have very narrow inhomogeneous distribution in bulk [18, 19] and, because of their inversion symmetry, can also have relatively narrow inhomogeneous distributions in nanostructures (< 15 GHz) [5]. Nanophotonic devices hosting two SiV^- centers with a sub-GHz difference between their transition frequencies have been reported [8], which is within our Stark tuning range. On this chip, we have also observed sub-GHz frequency detuning between two SnV^- centers (see Table I). The 1.7 GHz tuning range that we demonstrate in this Letter is large enough to overcome modest detunings between color centers and enable multi-emitter experiments.

The electric-field dependence of group-IV color centers can be harnessed in other schemes. Modulated electric fields have been proposed as an alternative way to overcome the inhomogeneous broadening of emitters [24, 33]. This approach would be particularly important for overcoming detunings between closely spaced emitters, for example if the emitters are in the same nanophotonic cavity [24, 33]. Spectral diffusion presents a challenge when working with group-IV color centers, which require resonant drive for optical spin initialization and control schemes. Feedback-based electric field tuning constitutes a tool for the dynamic stabilization of optical transition frequency of emitters [34].

All of these applications of Stark effect-based tuning can be made into more practical options by increasing the achievable Stark tuning range. The Stark tuning range can be further expanded by changing the electrode configuration to increase the field experienced by the emitter. Fabricating electrodes with a narrower gap between them would increase the applied field. Embedding the SnV^- center below the plane of the electrodes rather than in a nanopillar would increase the field experienced by the emitter a factor of 3. Furthermore, the tuning range can be increased by reducing the voltage-induced heating which allows the application of larger voltages.

In addition to contributing to a deeper understanding of the basic properties of SnV^- centers, our results pave the way for multi-emitter experiments based on group-IV color centers harnessing Stark shift tuning.

During the preparation of this manuscript, we became aware of a similar, very recent work [35].

ACKNOWLEDGMENTS

We are grateful to Daniil Lukin for his experimental assistance to this work. This work is financially supported by Army Research Office (ARO) (award no. W911NF-13-1-0309); National Science Foundation (NSF) RAISE TAQS (award no. 1838976); Air Force Office of Scientific Research (AFOSR) DURIP (award no. FA9550-16-1-0223). S.A. acknowledges support from Bloch postdoctoral fellowship in quantum science and engineer-

ing from Stanford Q-FARM. D.R. acknowledges support from the Swiss National Science Foundation (Project P400P2.194424). A.E.R. acknowledges support from the National Defense Science and Engineering Graduate (NDSEG) Fellowship Program, sponsored by the Air Force Research Laboratory (AFRL), the Office of Naval Research (ONR) and the Army Research Office (ARO).

C.D. acknowledges support from the Andreas Bechtolsheim Stanford Graduate Fellowship (SGF) and the Microsoft Research PhD Fellowship. Part of this work was performed at the Stanford Nanofabrication Facility (SNF) and the Stanford Nano Shared Facilities (SNSF), supported by the National Science Foundation under award ECCS-2026822.

-
- [1] H. J. Kimble, *Nature* **453**, 1023 (2008).
 - [2] S. Wehner, D. Elkouss, and R. Hanson, *Science* **362**, eaam9288 (2018).
 - [3] A. Sipahigil, R. E. Evans, D. D. Sukachev, M. J. Burek, J. Borregaard, M. K. Bhaskar, C. T. Nguyen, J. L. Pacheco, H. A. Atikian, C. Meuwly, R. M. Camacho, F. Jelezko, E. Bielejec, H. Park, M. Lončar, and M. D. Lukin, *Science* **354**, 847 (2016).
 - [4] A. E. Rugar, C. Dory, S. Aghaeimeibodi, H. Lu, S. Sun, S. D. Mishra, Z.-X. Shen, N. A. Melosh, and J. Vučković, *ACS Photonics* **7**, 2356 (2020).
 - [5] R. E. Evans, A. Sipahigil, D. D. Sukachev, A. S. Zibrov, and M. D. Lukin, *Physical Review Applied* **5**, 044010 (2016).
 - [6] N. H. Wan, T.-J. Lu, K. C. Chen, M. P. Walsh, M. E. Trusheim, L. De Santis, E. A. Bersin, I. B. Harris, S. L. Mouradian, I. R. Christen, E. S. Bielejec, and D. Englund, *Nature* **583**, 226 (2020).
 - [7] G. Thiering and A. Gali, *Physical Review X* **8**, 021063 (2018).
 - [8] R. E. Evans, M. K. Bhaskar, D. D. Sukachev, C. T. Nguyen, A. Sipahigil, M. J. Burek, B. Machielse, G. H. Zhang, A. S. Zibrov, E. Bielejec, H. Park, M. Lončar, and M. D. Lukin, *Science* **362**, 662 (2018).
 - [9] C. T. Nguyen, D. D. Sukachev, M. K. Bhaskar, B. Machielse, D. S. Levonian, E. N. Knall, P. Stroganov, R. Riedinger, H. Park, M. Lončar, and M. D. Lukin, *Physical Review Letters* **123**, 183602 (2019).
 - [10] M. K. Bhaskar, R. Riedinger, B. Machielse, D. S. Levonian, C. T. Nguyen, E. N. Knall, H. Park, D. Englund, M. Lončar, D. D. Sukachev, and M. D. Lukin, *Nature* **580**, 60 (2020).
 - [11] U. Wahl, J. G. Correia, R. Villarreal, E. Bourgeois, M. Gulka, M. Nesládek, A. Vantomme, and L. M. Pereira, *Physical Review Letters* **125**, 45301 (2020).
 - [12] A. E. Rugar, C. Dory, S. Sun, and J. Vučković, *Physical Review B* **99**, 205417 (2019).
 - [13] A. E. Rugar, H. Lu, C. Dory, S. Sun, P. J. McQuade, Z.-X. Shen, N. A. Melosh, and J. Vučković, *Nano Letters* **20**, 1614 (2020).
 - [14] T. Iwasaki, Y. Miyamoto, T. Taniguchi, P. Siyushev, M. H. Metsch, F. Jelezko, and M. Hatano, *Physical Review Letters* **119**, 253601 (2017).
 - [15] J. Görlitz, D. Herrmann, G. Thiering, P. Fuchs, M. Gandil, T. Iwasaki, T. Taniguchi, M. Kieschnick, J. Meijer, M. Hatano, A. Gali, and C. Becher, *New Journal of Physics* **22**, 013048 (2020).
 - [16] A. E. Rugar, S. Aghaeimeibodi, D. Riedel, C. Dory, H. Lu, P. J. McQuade, Z.-X. Shen, N. A. Melosh, and J. Vučković, *arXiv: 2102.11852* (2021).
 - [17] M. E. Trusheim, B. Pingault, N. H. Wan, M. Gündoğan, L. De Santis, R. Debroux, D. Gangloff, C. Purser, K. C. Chen, M. Walsh, J. J. Rose, J. N. Becker, B. Lienhard, E. Bersin, I. Paradeisanos, G. Wang, D. Lyzwa, A. R.-P. Montblanch, G. Malladi, H. Bakhru, A. C. Ferrari, I. A. Walmsley, M. Atatüre, and D. Englund, *Physical Review Letters* **124**, 023602 (2020).
 - [18] L. Rogers, K. Jahnke, T. Teraji, L. Marseglia, C. Müller, B. Naydenov, H. Schauffert, C. Kranz, J. Isoya, L. McGuinness, and F. Jelezko, *Nature Communications* **5**, 4739 (2014).
 - [19] A. Sipahigil, K. D. Jahnke, L. J. Rogers, T. Teraji, J. Isoya, A. S. Zibrov, F. Jelezko, and M. D. Lukin, *Physical Review Letters* **113**, 113602 (2014).
 - [20] S. Sun, J. L. Zhang, K. A. Fischer, M. J. Burek, C. Dory, K. G. Lagoudakis, Y.-K. Tzeng, M. Radulaski, Y. Kelaita, A. Safavi-Naeini, Z.-X. Shen, N. A. Melosh, S. Chu, M. Lončar, and J. Vučković, *Physical Review Letters* **121**, 083601 (2018).
 - [21] B. Machielse, S. Bogdanovic, S. Meesala, S. Gauthier, M. J. Burek, G. Joe, M. Chalupnik, Y. I. Sohn, J. Holzgrafe, R. E. Evans, C. Chia, H. Atikian, M. K. Bhaskar, D. D. Sukachev, L. Shao, S. Maity, M. D. Lukin, and M. Lončar, *Physical Review X* **9**, 031022 (2019).
 - [22] J. F. Ziegler, M. Ziegler, and J. Biersack, *Nuclear Instruments and Methods in Physics Research Section B: Beam Interactions with Materials and Atoms* **268**, 1818 (2010).
 - [23] P. Tamarat, T. Gaebel, J. R. Rabeau, M. Khan, A. D. Greentree, H. Wilson, L. C. L. Hollenberg, S. Prawer, P. Hemmer, F. Jelezko, and J. Wrachtrup, *Physical Review Letters* **97**, 083002 (2006).
 - [24] D. M. Lukin, A. D. White, R. Trivedi, M. A. Guidry, N. Morioka, C. Babin, Ö. O. Soykal, J. Ul-Hassan, N. T. Son, T. Ohshima, P. K. Vasireddy, M. H. Nasr, S. Sun, J.-P. W. MacLean, C. Dory, E. A. Nanni, J. Wrachtrup, F. Kaiser, and J. Vučković, *npj Quantum Information* **6**, 80 (2020).
 - [25] S. Meesala, Y.-I. Sohn, B. Pingault, L. Shao, H. A. Atikian, J. Holzgrafe, M. Gündoğan, C. Stavarakas, A. Sipahigil, C. Chia, R. Evans, M. J. Burek, M. Zhang, L. Wu, J. L. Pacheco, J. Abraham, E. Bielejec, M. D. Lukin, M. Atatüre, and M. Lončar, *Physical Review B* **97**, 205444 (2018).
 - [26] K. D. Jahnke, A. Sipahigil, J. M. Binder, M. W. Doherty, M. Metsch, L. J. Rogers, N. B. Manson, M. D. Lukin, and F. Jelezko, *New Journal of Physics* **17**, 043011 (2015).
 - [27] H. Bernien, L. Childress, L. Robledo, M. Markham, D. Twitchen, and R. Hanson, *Physical Review Letters* **108**, 043604 (2012).
 - [28] A. Sipahigil, M. L. Goldman, E. Togan, Y. Chu, M. Markham, D. J. Twitchen, A. S. Zibrov, A. Kubanek, and M. D. Lukin, *Physical Review Letters* **108**, 143601 (2012).

- (2012).
- [29] R. Lettow, Y. L. Rezus, A. Renn, G. Zumofen, E. Ikonen, S. Götzinger, and V. Sandoghdar, *Physical Review Letters* **104**, 26 (2010), arXiv:0911.3031.
 - [30] R. B. Patel, A. J. Bennett, I. Farrer, C. A. Nicoll, D. A. Ritchie, and A. J. Shields, *Nature Photonics* **4**, 632 (2010).
 - [31] E. Flagg, A. Muller, S. Polyakov, A. Ling, A. Migdall, and G. Solomon, *Physical Review Letters* **104**, 137401 (2010), arXiv:1004.0153.
 - [32] M. Pompili, S. L. N. Hermans, S. Baier, H. K. C. Beukers, P. C. Humphreys, R. N. Schouten, R. F. L. Vermeulen, M. J. Tiggelman, L. d. S. Martins, B. Dirkse, S. Wehner, and R. Hanson, arXiv: 2102.04471 (2021).
 - [33] R. Trivedi, A. White, S. Fan, and J. Vučković, *Physical Review A* **102**, 033707 (2020).
 - [34] V. M. Acosta, C. Santori, A. Faraon, Z. Huang, K.-M. C. Fu, A. Stacey, D. A. Simpson, K. Ganesan, S. Tomljenovic-Hanic, A. D. Greentree, S. Praver, and R. G. Beausoleil, *Physical Review Letters* **108**, 206401 (2012).
 - [35] L. De Santis, M. Trusheim, K. Chen, and D. Englund, arXiv: 2102.01322 (2021), arXiv:2102.01322.